Available online at www.sciencedirect.com

SciVerse ScienceDirect

Acta Materialia 61 (2013) 2113–2120

Acta MATERIALIA

www.elsevier.com/locate/actamat

Texture and training of magnetic shape memory foam

Cassie Witherspoon [a,1], Peiqi Zheng [b], Markus Chmielus [a,2], Sven C. Vogel [c], David C. Dunand [b], Peter Müllner [a,*]

[a] Department of Materials Science and Engineering, Boise State University, Boise, ID 83725, USA
[b] Department of Materials Science & Engineering, Northwestern University, Evanston, IL 60208, USA
[c] LANSCE, Los Alamos National Laboratory, Los Alamos, NM 87545, USA

Received 30 September 2012; received in revised form 22 December 2012; accepted 24 December 2012
Available online 29 January 2013

Abstract

Magnetic shape memory alloys display magnetic-field-induced strain (MFIS) of up to 10% as single crystals. Polycrystalline materials are much easier to create but display a near-zero MFIS because twinning of neighboring grains introduces strain incompatibility, leading to high internal stresses. Pores reduce these incompatibilities between grains and thus increase the MFIS of polycrystalline Ni–Mn–Ga, which after training (thermo-magneto-mechanical cycling) exhibits MFIS as high as 8.7%. Here, we show that this training effect results from a decoupling of struts surrounding pores in polycrystalline Ni–Mn–Ga during the martensitic transformation. To show this effect in highly textured porous samples, neutron diffraction measurements were performed as a function of temperature for phase characterization and a method for structure analysis was developed. Texture measurements were conducted with a magnetic field applied at various orientations to the porous sample, demonstrating that selection of martensite variants takes place during cooling.

Keywords: Martensitic phase transformation; Neutron diffraction; Thermal cycling; Ni_2MnGa; Heusler alloys

1. Introduction

Magnetic shape memory alloys (MSMAs) have gained much attention due to the large reversible strain which can be induced in single crystals by varying the direction of a magnetic field [1]. Off stoichiometric monocrystalline Ni–Mn–Ga MSMAs, in particular, are very promising as they show strains up to 10% near room temperature [2–6]. The strain is produced by twin boundary motion, which is induced by a change of orientation of a magnetic field [1,3,7–9]. In the martensite phase, Ni–Mn–Ga has a high magneto-crystalline anisotropy, which provides the driving force for twin variant growth through twin boundary motion [6,10,11]. Many studies have investigated the parameters controlling twin mobility. Surface defects pin twin boundaries, requiring additional force to unpin the twins such that further deformation can occur [12–14]. Non-metallic impurities (as particles or in solid solution) also pin twin boundaries and thus increase the twinning stress [15]. The higher the twinning stress, the lower the driving force that can be imposed magnetically against an external load [15]. The twin density, hierarchically twinned microstructures and conjugate twinning have a significant impact on twin mobility and possibly affect the fatigue life of magnetic actuation [8,10,15–17]. Training (thermo-magneto-mechanical cycling (TMC)) leads to martensite variant selection of preferentially oriented variants, which reduces the twinning stress, for further cycles, in single crystals [3,4,10,12,18].

Recently, we have shown that the MFIS of polycrystalline Ni–Mn–Ga can be significantly increased by introducing porosity [19–22]. Pores replace grain boundaries and reduce internal constraints imposed by the misorientation

* Corresponding author. Tel.: +1 208 426 5136.
E-mail address: PeterMullner@BoiseState.edu (P. Müllner).
[1] Present address: Micron Technology Inc., Boise, ID, USA.
[2] Present address: Department of Materials Science and Engineering, Cornell University, Ithaca, NY 14853, USA.

1359-6454/$36.00
http://dx.doi.org/10.1016/j.actamat.2012.12.032

of neighboring crystals. Polycrystalline porous Ni–Mn–Ga xwith a bimodal pore size distribution (hereafter "bimodal foam") have shown very large MFIS of up to 8.7% [20,21]. A bimodal foam consists of struts connected at nodes forming a network surrounding the larger (500–600 μm) pores; these struts and pores contain smaller (75–90 μm) pores. The MFIS of 8.7% of these hierarchically porous bimodal foams is higher than expected for a randomly textured foam with twin boundary motion as the sole source of deformation within a strut. We have suggested that the high MFIS may be due to texture (a crystallographic effect) [20] and/or strut hinging (a geometric effect) [21]. Even if the foam were a single crystal, that would already have been a breakthrough as such a "single crystal foam" would be much easier to make than a bulk single crystal. In the case of strut hinging, struts tilt with the tilt axis passing through the node [23]. With hinging produced by twin boundary motion within the node, localized bending strain at the node could lead to large displacements further away from the hinge and therefore produce large macroscopic strains.

Neutron diffraction was employed here to identify the active mechanisms of deformation and training within the bimodal foams. Neutron diffraction was chosen due to the high interaction volume of neutrons, making it possible to observe changes in microstructure within the sample. Because the samples are oligocrystalline (they contain a small number of grains), we apply a method rarely used for neutron diffraction, but well-known in X-ray powder diffraction, namely spinning the sample to provide a better powder average of its crystal structure; this method makes structure analysis for highly textured and/or oligocrystalline materials possible.

2. Experimental procedures

Samples of similar foam studied previously [19,21] were used here, and only a summary of the foam processing is given below. High purity elements (99.9% nickel pellets from ESPI, 99.999% gallium pellets from Alfa Aesar and electrolytic-purity manganese flakes from Alfa Aesar), forming an alloy with a nominal composition of $Ni_{52}Mn_{24.3}Ga_{23.7}$, with melting point slightly above 1100 °C [24], were melted in a vacuum induction furnace (Reitel, Induret Compact) and cast into ingots within copper molds. Open-cell bimodal foams were created via the replication casting method: an ingot was remelted and the melt was pressure infiltrated into a preform consisting of a blend of sodium aluminate ($NaAlO_2$) powders with bimodal size distribution. These powders were then removed by sonication in 34% H_2SO_4 and subsequently in 10% HCl, which leads to partial strut thinning. The resulting polycrystalline $Ni_{52}Mn_{24.3}Ga_{23.7}$ foam was chemically homogenized (1000 °C/1 h) in vacuum and subjected to a stepwise heat treatment to establish the $L2_1$ structure (725 °C/2 h, 700 °C/10 h, 500 °C/20 h).

Neutron diffraction experiments were conducted at the HIPPO beam line of the Los Alamos Neutron Science Center (LANSCE) with the time-of-flight method using a 10 mm diameter neutron beam from a tungsten spallation source. Details of the HIPPO beamline, including the available detector banks and their d-spacing ranges, are reported in Ref. [25]. Neutron diffraction experiments were done in a magnetic field using a cylindrical sample (referred to as sample 1) with a diameter of 9 mm, a height of 7.85 mm and a porosity of $62.4 \pm 0.5\%$ as determined by measurements of mass and volume. A small irregular shaped sample (sample 1a) ~3 mm thick was cut from sample 1. Diffraction experiments for crystal structure analysis were performed on sample 1a in a cryostat at controlled temperatures of 203 K (purely martensitic) and 320 K (purely austenitic).

For temperature-controlled diffraction experiments without applied magnetic field, sample 1a was rotated to four orientations to measure texture at 203 and 320 K. In addition, the sample was rotated to 61 different sample orientations to get a powder average permitting structure analysis using GSAS software [26,27]. Texture was analyzed with the MAUD Rietveld analysis software [28,29].

For diffraction experiments with an applied magnetic field, sample 1 was glued to an aluminum rod. A magnetic field of 1 T was produced with an electromagnet. The aluminum rod was connected to a gear controlling inclination about the x direction (Fig. 1a). Before conducting neutron diffraction, the sample was heated, at zero magnetic field strength, to 40 °C via heating the aluminum rod to produce the austenite phase. At 40 °C, the magnetic field was turned on and the sample was cooled in the magnetic field to 5 °C to ensure the sample was in the martensite phase. Cooling and heating were achieved with a chilled water copper coil and a resistive heating element inserted into the aluminum rod, respectively. The magnetic field was applied parallel to the z direction, which coincided with the axis of the foam cylinder.

Diffraction measurements were taken with the sample z-axis forming an angle of 0°, 45° and 90° with respect to the magnetic field, as illustrated in Fig. 1b. To get texture information for each of these angles, four sample orientations relative to the beam were needed. To get the four orientations for the texture measurement at a constant mutual orientation of magnetic field direction and sample, the whole magnet stage was rotated inside the sample chamber. The four orientations of the stage relative to the beam are illustrated in Fig. 1c by four lines marked 1–4. Thus, 12 diffraction experiments were performed at a given temperature, i.e., one diffraction experiment at each of the four stage orientations for each of the three sample orientations relative to the magnetic field. The first series of diffraction experiments was performed at 5 °C on sample 1 cooled without applied magnetic field (i.e. in the untrained state). Then the sample was heated to 40 °C, which is above the austenite finish temperature, and a second series of four stage orientation diffraction experiments was conducted

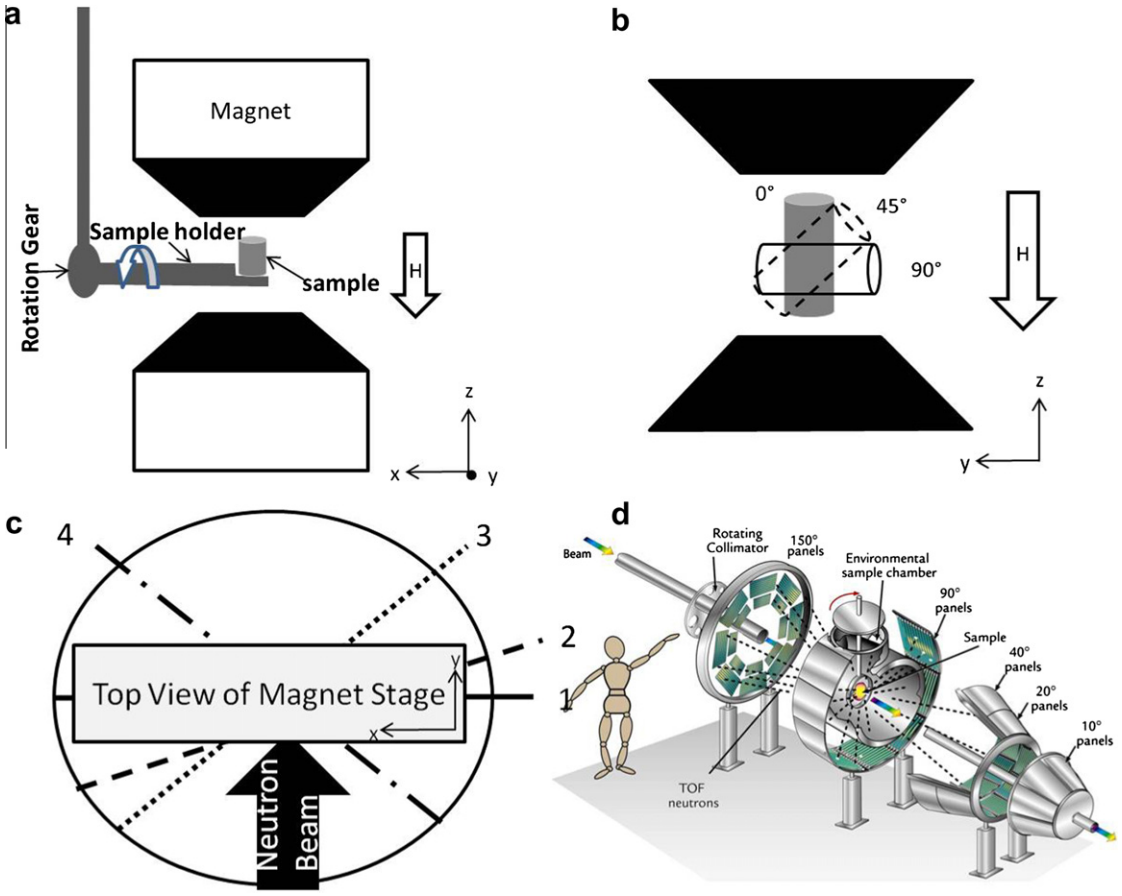

Fig. 1. Experimental setup of diffraction experiments with magnetic field applied. (a) Electromagnet with pole pieces (black) and the direction of the magnetic field, the sample holder and rotation gear, and the sample centered between the pole pieces. The sample was rotated about the x direction. (b) The three sample orientations relative to the magnetic field 0° (gray), 45° (dashed black), and 90° (solid black). (c) The four magnet stage orientations used for the texture experiments with a magnetic field. The stage orientation 1 was used as the 0° reference so that stage orientation 2 was +20°, stage orientation 3 was +40° and stage orientation 4 was −40°. (d) HiPPO diffractometer at LANSCE.

(at only one sample orientation because of the cubic symmetry of the austenite phase). With the magnetic field turned on, the foam was then cooled to 5 °C, which is below the martensite finish temperature. Following the field cooling a third series of 12 diffraction experiments was conducted. The last two temperature steps and accompanying neutron scans were then repeated one more time.

Prior to the neutron diffraction experiments, the sample was exposed to a rotating magnetic field of 0.97 T for measuring MFIS. During field rotations, the samples were subjected to TMC, by heating and cooling through the phase transformation. TMC allows for simultaneous observation of the phase transformation, thermo-magneto-mechanical training and measurement of MFIS produced by a sample in a fully martensitic state. Heating and cooling of the sample was achieved by convective heat transfer with hot and cold air in the sample chamber. The sample temperature was measured with a thermocouple in direct contact with the sample. The temperature was averaged over one revolution of the magnetic field, and the maximum MFIS for one magnet revolution was plotted against the temperature. The detection limit of MFIS in the TMC experiment was 0.01% for experiments with variable temperature and 0.002% for experiments at constant ambient temperature. The larger experimental error in experiments with variable temperature originated from the forced air flow. A detailed description of the TMC experiment is given in Ref. [21].

3. Results

3.1. Neutron diffraction

Fig. 2 shows diffraction spectra of sample 1a taken at 203 K from the integrated 90° detector ring (Fig. 1d) for four selected sample orientations (Fig. 2a) and for all 61 sample orientations (Fig. 2b). The integrated data from 61 orientations (Fig. 2b) showed additional peaks 0 2 0 and 1 0 5 for d spacing between 2.5 and 3.0 Å, which permitted to refine the structure. Peaks at d spacing smaller than 1.5 Å were not indexed because several high-index poles match these peaks within experimental error, their intensity was low and did not significantly change during training. With the GSAS software, the data recorded at 203 K were fitted to the various martensite structures,

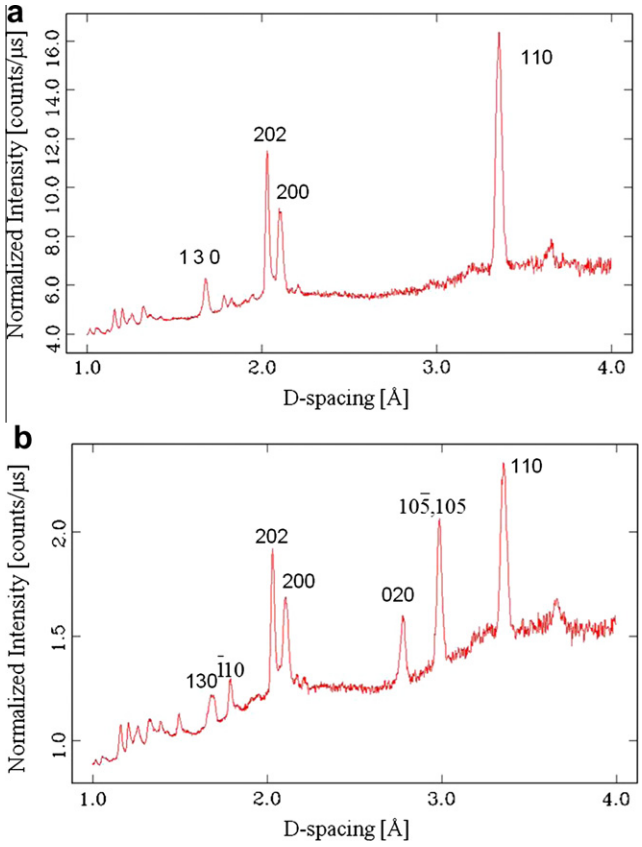

Fig. 2. Effect of additional sample orientations on powder average of the crystal structure from the small sample 1a with temperature controlled environment. Diffraction data integrated and averaged for the whole 90° detector ring for (a) four sample orientation and (b) 61 sample orientations.

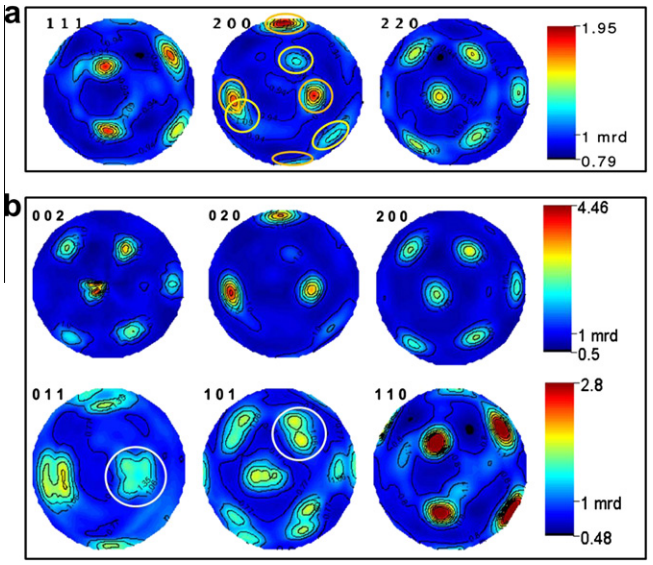

Fig. 3. Pole figures of sample 1a (a) at 320 K corresponding to the austenite phase of Ni–Mn–Ga and (b) at 203 K corresponding to the 10M martensite phase of Ni–Mn–Ga. The martensite is indexed according to the 10M axis system.

including the non-modulated tetragonal (NM), and modulated 10M and 14M structures. The data recorded at 300 K were fitted to the cubic $L2_1$ structure of the austenite phase [10,11,30–34]. The 10M structure (space group $I2/M$) provided the best fit for the martensite with the lattice parameters $a = 4.221$, $b = 5.527$, $c = 20.952$ Å and $\beta = 90.209°$. The austenite had a face-centered cubic (fcc) structure with a lattice parameter 5.812 Å. The structure found from spinning the sample in the cryostat was then used to fit texture with the MAUD software.

The pole figures for austenite (Fig. 3a) show a sharp texture with two dominant crystal orientations, circled in orange and yellow in the 200 pole figure. This indicates an orientation distribution similar to a bi-crystal. When comparing the martensite texture (Fig. 3b) with the austenite texture (Fig. 3a), the *b*-axis of the martensite corresponds to one of the *a*-axis in the austenite. The 011, 101, and 110 pole figures of the martensite phase show a splitting of the peaks, indicating the formation of many martensite variants. This effect is particularly strong in the 011 and 101 pole figures of the martensite, indicated by circles in Fig. 3b.

Neutron diffraction spectra for the sample subjected to the magnetic field show an intensity shift before and after thermo-magnetic training. Fig. 4 shows the diffraction pattern integrated from four sample orientations for the whole backscatter detector ring after cooling without magnetic field (Fig. 4a) and after cooling with a magnetic field of 1 T (Fig. 4b). After in-field cooling (training), the 020 peak dropped to about half its intensity, as compared to the strongest 105 peak. In contrast, the 103 peak increased as compared to the 020 peak. Furthermore, the 215 and 1,1,10 peaks were reduced to a near-zero intensity in Fig. 4b for field cooling.

3.2. Magnetomechanical properties

The magneto-mechanical behavior of sample 1 during heating and cooling is shown in Fig. 5. During the initial heating (black squares in Fig. 5), the MFIS remained constant at 0.4% from 20 to 40 °C. At 41 °C the martensite-to-austenite transformation started, resulting in a rapid decrease of MFIS to 0.1% at 42 °C. Upon subsequent cooling, the strain increased back to 0.4% from 24 to 18 °C. During this first heating/cooling (H/C 1) cycle, the temperature was raised from 18 to 42 °C within less than 2 min, such that the sample temperature did not equilibrate at 42 °C. Thus, the sample might have had some retained martensite phase at this temperature, explaining the relatively large 0.1% MFIS. The second heating/cooling (H/C 2, open circles in Fig. 5) cycle started at 22 °C with a lower MFIS at 0.3%, probably due to an incomplete transformation, i.e. the remaining austenite phase suppressed large deformation. The strain gradually decreased from 0.3 to near 0% (below the resolution limit of 0.01%) during heating from 28 to 36 °C, with a spike in MFIS at 35 °C during the phase transformation. On the cooling part of

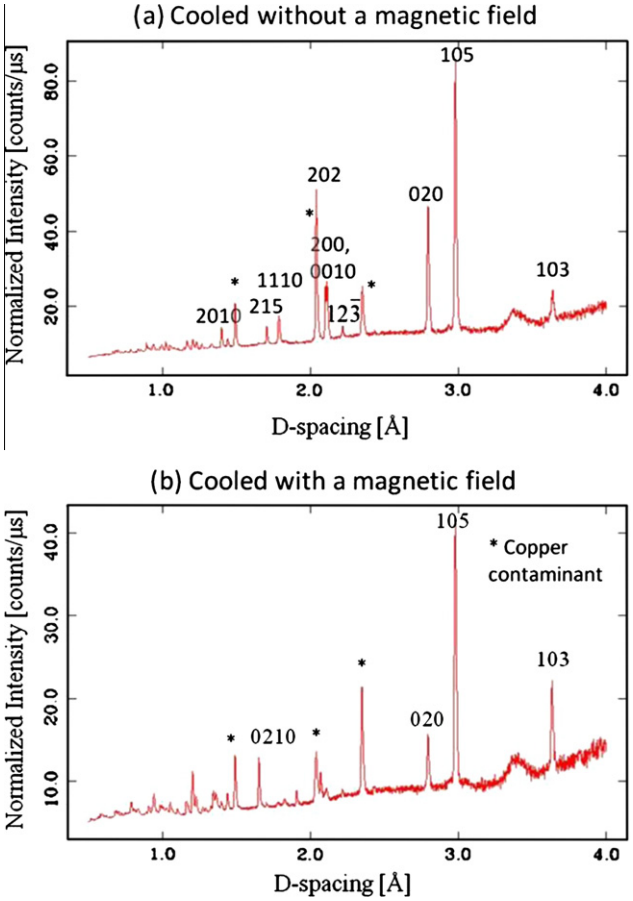

Fig. 4. Neutron back-scattered diffraction spectra at 278 K for samples which had been cooled (a) without a magnetic field and (b) with a magnetic field of 1 T. The intensities were integrated from four sample orientations. The 10M monoclinic axis system was used for indexing. Cooling in the magnetic field (training) increased the 103 and 0210 reflections and decreased the 020 and 202 reflections. The copper cooling tubes were partially in the beam, so that some copper peaks are convoluted with the Ni–Mn–Ga peaks (e.g. at 2.0 Å *d* spacing).

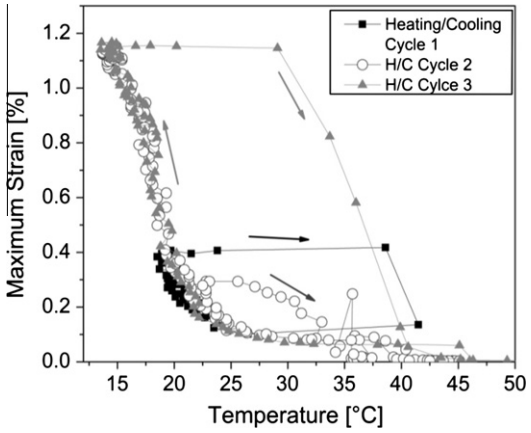

Fig. 5. Plot of MFIS vs. temperature during the three thermo-magneto-mechanical cycles of sample 1. Arrows indicate the direction of temperature change.

this second cycle, the temperature was lowered to 14 °C and the MFIS increased to 1.15%. On the third heating (H/3, gray triangles in Fig. 5), the strain remained constant at 1.15% up to 30 °C, above which it dropped to near 0% at 42 °C. On the third cooling, the austenite-to-martensite transformation occurred from 22 to 14 °C. The final MFIS at 14 °C was again 1.15%. At the lowest temperature of 14 °C, the MFIS did not exhibit a plateau, indicating that the martensitic transformation is not complete at this temperature and that higher MFIS might be possible at lower temperatures.

4. Discussion

4.1. Magnetomechanical properties

Upon TMC, the sample showed an almost threefold increase in MFIS from 0.4% (H/C1) to 1.15% (H/C 2 and 3), reflecting the training effect (Fig. 5) [21]. When rotating a magnetic field during heating and cooling, the magnetic field favors two particular twin variants sharing a mobile twin boundary. Twin variants which are not contributing to the MFIS do not form. Thus, twin–twin interactions that reduce twin mobility are eliminated [16,18,21,35]. During H/C 1, the temperature change was so fast that the foam probably did not transform completely to austenite, resulting in a strain of 0.1% at the highest temperature, instead of a near zero value expected for the austenite phase. The incomplete transformation may have generated interacting twinning systems, thus lowering the initial strain seen in H/C 2. However, by fully heating to austenite in H/C 2, the incompatible twins were eliminated as demonstrated by the tripling in MFIS during the second cooling (Fig. 5). Sample 1 also notably showed a MFIS of 1.15%, which is very large as compared to other textured non-porous polycrystals [36,37]. If each strut can transform individually, then during training the martensite orientation can be trained in each strut individually without the constraints of the bulk. Assuming that struts (rather than nodes) are responsible for most of the MFIS in the foam, then, being able to individually train each strut would make the foam much more responsive to any kind of training methods. In other textured bulk polycrystals that were mechanically trained, the strain increase due to mechanical training was only 0.2%, [36–38]. By contrast, some foams have shown much more significant strain increases associated with thermo-magneto-mechanical training, e.g. from 0.75% to 8.7% [21]. A quantitative understanding of training effects explaining why training is more effective in some foams than in others requires more experiments and is beyond the scope of this study.

4.2. Texture analysis

The 111 austenite pole figure in Fig. 3a correlates with the 110 martensite pole figure in Fig. 3b. Similarly, the 200 and 220 pole figures of austenite correlate with 020 and

200 of martensite. This correlation confirms the orientation relationship $(110)_M//\{111\}_A$, $(100)_M//\{110\}_A$, $(010)_M//\{100\}_A$ and $(001)_M//\{110\}_A$. The splitting of peaks in the 011 and 101 martensite pole figures (Fig. 3b) is typical of martensite twin variant formation [39]. However, twin variant formation in bulk single crystals has been shown to cause pole splitting from the 200 and 110 type martensite poles [39]. In the present foam, peak splitting did not appear in the 200 pole figures. The Bain strain of the phase transformation is parallel to $\langle 100\rangle$, such that the lattice distortion may be more easily shown by the 110 type poles [40]. During the phase transformation, if expansion of the unit cell is parallel to the [100] direction the (100) pole does not change orientation. However, any other crystallographic plane not parallel to the expansion of the lattice would demonstrate a change in the orientation of the plane normal. If each strut is allowed to transform individually, such as in a single unit cell, the pole splitting caused by the Bain strain would be more easily detectable for {110} planes. In a bulk sample the martensitic transformation is constrained by the surrounding material. To overcome this constraint the material twins on multiple twinning planes. This causes the pole splitting of the {100} and {110} martensite poles. If each strut transforms individually without the constraint or influence of the neighboring material, one would expect to see the pole splitting only in particular pole figures because not all twin variants would be produced as the result of the transformation [41]. If on the other hand all struts of a given crystallographic orientation transformed simultaneously and in the exact same manner, the localized stress would act as a constraint on the transformation. In this case twinning on several twinning systems would be required to make the phase transformation favorable. In this case, a higher degree of pole splitting would be expected. Thus, the existence of poles without pole splitting indicates that struts are mechanically decoupled such that they can transform freely with little twinning. Decoupling may be achieved via several mechanisms: (i) fracture of struts is the most evident but was not detected; (ii) hinging would result in large strain with only little twinning localized at the neck of the struts; (iii) if the twinning stress becomes low enough, differently oriented struts can strain to large amounts and adapt to the strain of neighboring struts. Variant selection via thermo-magnetic cycling (Fig. 5) is hindered when multiple twinning systems are formed during the martensitic transformation. If the internal constraints within the foam are limited to the nodes, the absence of grain boundaries in the struts would allow the struts to freely transform. The two dominant crystal orientations were found in the austenite pole figures (Fig. 3a), suggesting that there are probably two dominant crystal orientations in sample 1a, suggesting grains are on the millimeter size range. The size of the grains also increases the chance that struts are monocrystalline, as the grain boundary volume decreases with increasing grain size.

The martensite variant selection can be inferred from the intensity shifts in Fig. 4. In a strongly textured sample, some reflections hkl disappear because no corresponding planes fulfill the Bragg condition. For different martensite variants of the same parent grain, corresponding planes (hkl) form a large angle. For one variant, (hkl) may fulfill the Bragg condition for a given sample/beam geometry while for another variant, this may not be the case. The strong intensity shifts of several peaks between cooling with and without magnetic field are therefore a signature of magnetic-field-induced variant selection [41,42], which is a training mechanism.

Pole figures before and after field cooling at the different sample orientations to the field could not be generated, probably because of the presence of magnetic scattering which at present cannot be modeled for texture analysis with available Rietveld codes. Only the initial experiment with cooling to 5 °C, in the magnet sample holder, without an applied field generated a texture fit. All attempts at texture refinement with a field failed to result in pole figures. Glavatskyy and co-authors [43] did neutron experiments to study the temperature-dependent, magnetic scattering contribution in Ni–Mn–Ga without applying a magnetic field during the scattering experiment. They found that at 200 K there was a small contribution of magnetic scattering. They also suggest that anisotropic lattice expansion changes the magnetic interaction of neighboring atoms and results in discontinuous increase of the magnetic scattering character with temperature. Fitting of texture of the martensite in the cryostat was possible due to the absence of a magnetic field, leaving only the much weaker ordering of magnetic moments due to temperature at 200 K [43,44]. Texture was only difficult to fit when the sample was exposed to a magnetic field. This suggests that there are different local strains and magnetic scattering both contributing to the total intensity [36,45]. The transverse magnetostriction constant changes sign when cooling from austenite to martensite [46]. This reversal contributes to the difficulty of conducting texture analysis and structure refinement for polycrystalline and single crystalline magnetic shape memory alloys. The reversal has been reported elsewhere for neutron diffraction, possibly indicating the importance of the magnetic scattering [44,47,48].

4.3. Structure analysis

There are many methods for evaluating structure in single crystals, such as powdering the specimen (destructive) or using a goniometer to rotate the sample to many different orientations [49–51]. For fine-grained bulk polycrystals, crystal structure refinement can usually be easily achieved. Texture fitting analysis methods work well on fine-grained materials or materials with a weak texture yet fail for large-grained or sharply textured materials where peaks may be entirely absent from the diffraction pattern as is the case in Fig. 2 [52]. Fig. 2 shows diffraction data from the integrated 90° detector ring (Fig. 1d) for all four sample

orientations (Fig. 2a) and 61 sample orientations (Fig. 2b). A larger number of sample orientations, in essence "spinning" (though in discrete steps) to give a powder average of the crystal structure, show additional diffraction peaks, as compared to the standard four orientations. Therefore, the spinning method can help bridge the gap of analysis methods between mono- and polycrystals and make structure and texture analysis for samples with large grains or sharp textures easier.

5. Conclusions

Neutron diffraction measurements were performed on polycrystalline Ni–Mn–Ga foams with bimodal pore size distribution as a function of temperature for phase characterization. A method for structure analysis was developed which is useful for oligocrystalline samples and samples with strong texture. Texture measurements were conducted with a magnetic field applied at various orientations to the sample, demonstrating that selection of martensite variants took place. The following main results were obtained:

1. Crystal structures for the austenite and martensite phases were identified and their texture analyzed at two temperatures, one in the austenite and one in the martensite region. The resulting pole figures show a very sharp texture and are consistent with previously reported orientation relationships.
2. Spinning the sample during diffraction gives a better powder average of the crystal structure and allows for structure analysis for sharp textures. Spinning may be used for structure analysis of large-grained or sharply textured materials. Difficulties in texture refinement when a magnetic field is applied suggest that the contribution of the magnetic order induced by the magnetic field is too strong to be neglected. Present Rietveld software allowing texture analysis needs to be extended to also include the magnetic contributions.
3. A training effect was observed by diffraction peak intensity changes before and after field cooling. The sample also showed a training effect by an increase in MFIS from 0.4% to 1.15% before and after TMC. This large training effect is attributed to struts being mechanically decoupled during the martensitic transformation.

Acknowledgments

This project was funded by the National Science Foundation through grant NSF-DMR 1207192 (Boise State University) and DMR-1207282 (Northwestern University). M.C. acknowledges partial financial support through the German Research Foundation (DFG) priority program SPP 1239 (grant No. Schn 1106/1). P.M. is thankful to ETH Zürich for donating magneto-mechanical testing devices. This work has benefited from the use of the Lujan Neutron Scattering Center at LANSCE, which is funded by the US Department of Energy's Office of Basic Energy Sciences. Los Alamos National Laboratory is operated by Los Alamos National Security LLC under DOE contract DE-AC52-06NA25396.

References

[1] Ullakko K, Huang JK, Kantner C, O'Handley RC, Kokorin VV. Appl Phys Lett 1996;69:1966.
[2] Chernenko VA, Cesari E, Kokorin VV, Vitenko IN. Scripta Metall Mater 1995;33:1239.
[3] Müllner P, Chernenko VA, Kostorz G. J Appl Phys 2004;95:1531.
[4] Müllner P, Chernenko VA, Wollgarten M, Kostorz G. J Appl Phys 2002;92:6708.
[5] Murray SJ, Marioni M, Allen SM, O'Handley RC, Lograsso TA. Appl Phys Lett 2000;77:886.
[6] Sozinov A, Likhachev AA, Lanska N, Ullakko K. Appl Phys Lett 2002;80:1746.
[7] Müllner P, Chernenko VA, Kostorz G. Scripta Mater 2003;49:129.
[8] Müllner P, King AH. Acta Mater 2010;58:5242.
[9] Ullakko K, Huang JK, Kantner C, Kokorin VV, O'Handley RC. J Appl Phys 1997;81:5416.
[10] Müllner P, Mukherji D, Aguirre M, Erni R, Kostorz G. In: Howe JM, Laughlin DE, Lee JK, Dahmen U, Soffa WA, editors. Solid-to-solid phase transformations in inorganic materials, vol. 2. Warrendale (PA): TMS; 2005. p. 171.
[11] Sozinov A, Likhachev AA, Ullakko K. IEEE Trans Magn 2002;38:2814.
[12] Chmielus M, Glavatskyy I, Hoffmann J-U, Chernenko VA, Schneider R, Müllner P. Scripta Mater 2011;64:888.
[13] Chmielus M, Rolfs K, Wimpory R, Reimersr W, Müllner P, Schneider R. Acta Mater 2010;58:3952.
[14] Chmielus M, Witherspoon C, Ullakko K, Müllner P, Schneider R. Acta Mater 2011;59:2948.
[15] Straka L, Lanska N, Ullakko K, Sozinov A. Appl Phys Lett 2010;96:131903.
[16] Aalito I, Soroka A, Ge Y, Söderberg O, Hannula S-P. Smart Mater Struct 2010;19:075014.
[17] Kustov S, Pons J, Cesari E, Van Humbeeck J. Acta Mater 2004;52:3075.
[18] Chmielus M, Chernenko VA, Knowlton WB, Kostorz G, Müllner P. Euro Phys J S T 2008;158:79.
[19] Boonyongmaneerat Y, Chmielus M, Dunand DC, Müllner P. Phys Rev Lett 2007;99:247201.
[20] Chmielus M, Witherspoon C, Wimpory RC, Paulke A, Hilger A, Zhang X, et al. J Appl Phys 2010;108:123526.
[21] Chmielus M, Zhang XX, Witherspoon C, Dunand DC, Müllner P. Nat Mater 2009;8:863.
[22] Zhang XX, Witherspoon C, Müllner P, Dunand DC. Acta Mater 2011;59:2229.
[23] Gibson LJ, Ashby MF. Cellular solids structure and properties. 2nd ed. Cambridge: Cambridge University Press; 1997.
[24] Schlagel DL, Wu YL, Zhang W, Lograsso TA. J Alloys Compd 2000;312:77.
[25] Wenk HR, Lutterotti L, Vogel S. Nucl Instr Meth Phys Res 2003;515:575.
[26] Larson AC, Von Dreele RB. Los Alamos National Laborartory Report LAUR 2004;86:748.
[27] Vogel SC. J Appl Cryst 2011;44:873.
[28] Lutterotti L, Matthies S, Wenk HR. In: MAUD (Material analysis using diffraction): a user friendly Java program for Rietveld texture analysis and more; 1999. p. 1599.
[29] Wenk HR, Lutterotti L, Vogel S. Nucl Instr Meth Phys Res A 2003;515:575.
[30] Pons J, Chernenko VA, Santamarta R, Cesari E. Acta Mater 2000;48:3027.

[31] Pons J, Santamarta R, Chernenko VA, Cesari E. Mater Chem Phys 2003;81:457.
[32] Pons J, Santamarta R, Chernenko VA, Cesari E. Mater Sci Eng A 2006;438–440:931.
[33] Richard M, Feuchtwanger J, Schlagel D, Lograsso T, Allen SM, O'Handley RC. Scripta Mater 2006;54:1797.
[34] Righi L, Albertini F, Pareti L, Paoluzi A, Calestani G. Acta Mater 2007;55:5237.
[35] Chulist R, Skrotzki W, Oertel CG, Böhm A, Pötschke M. Scripta Mater 2010;63:548.
[36] Gaitzsch U, Pötschke M, Roth S, Rellinghaus B, Schultz L. Acta Mater 2009;57:365.
[37] Pötschke M, Weiss S, Gaitzsch U, Cong D, Hürrich C, Roth S, et al. Scripta Mater 2010;63:383.
[38] Gaitzsch U, Pötschke M, Roth S, Rellinghaus B, Schultz L. Scripta Mater 2007;57:493.
[39] Kaufmann S, Rössler UK, Heczko O, Wuttig M, Buschbeck J, Schultz L, et al. Phys Rev Lett 2010;104:145702.
[40] Richard ML, Feuchtwanger J, Allen SM, O'Handley RC, Lázpita P. Metall Mater Trans A 2007;38:777.
[41] Wang YD, Ren Y, Li H, Choo H, Benson ML, Brown DW, et al. Adv Mater 2006;18:2392.
[42] Wang G, Wang YD, Ren Y, Liu Y, Liaw PK. Metall Mater Trans A 2009;39:3184.
[43] Glavatskyy I, Glavatska N, Urubkov I, Hoffman JU, Bourdarot F. Mater Sci Eng A 2008;481–482:298.
[44] Lázpita P, Barandiaran JM, Gutiérrez J, Richard M, Allen SM, O'Handley RC. Euro Phys J S T 2008;158:6.
[45] Nie ZH, Wang YD, Wang GY, Richardson JW, Wang G, Liu YD, et al. Metall Mater Trans A 2008;39:3113.
[46] Barandiarán JM, Chernenko VA, Gutiérrez J, Orúe I, Lázpita P. Appl Phys Lett 2012;100:262410.
[47] Richard ML, Feuchtwanger J, Allen SM, O'Handley RC, L'azpita P, Barandiaran JM, et al. Philos Mag 2007;87:3437.
[48] Stebner A, Gao X, Brown DW, Brinson LC. Acta Mater 2011;59:2841.
[49] Ihringer J, Küster A. J Appl Chrust 1993;26:135.
[50] Creagh DC, Foran GJ, Cookson DJ, Garrett RF, Johnson F. J Synch Rad 1998;5:823.
[51] Margulies L, Kramer MJ, McCallum RW, Kycia S, Haeffer DR, Lang JC, et al. Rev Sci Instr 1999;70:3554.
[52] Xie Y, Lutterotti L, Wenk HR, Kovacs F. J Mater Sci 2004;39:3329.